Neoadjuvant Chemotherapy Induces Genomic and Transcriptomic Changes in Ovarian Cancer

Melissa Javellana[1], Mark A. Eckert[1], Janna Heide[1], Katarzyna Zawieracz[1], Melanie Weigert[1], Sarah Ashley[1], Elizabeth Stock[1], David Chapel[2], Lei Huang[3], S. Diane Yamada[1], Ahmed Ashour Ahmed[4,5], Ricardo R. Lastra[2], Mengjie Chen[3], and Ernst Lengyel[1]

ABSTRACT

The growing use of neoadjuvant chemotherapy to treat advanced stage high-grade serous ovarian cancer (HGSOC) creates an opportunity to better understand chemotherapy-induced mutational and gene expression changes. Here we performed a cohort study including 34 patients with advanced stage IIIC or IV HGSOC to assess changes in the tumor genome and transcriptome in women receiving neoadjuvant chemotherapy. RNA sequencing and panel DNA sequencing of 596 cancer-related genes was performed on paired formalin-fixed paraffin-embedded specimens collected before and after chemotherapy, and differentially expressed genes (DEG) and copy-number variations (CNV) in pre- and post-chemotherapy samples were identified. Following tissue and sequencing quality control, the final patient cohort consisted of 32 paired DNA and 20 paired RNA samples. Genomic analysis of paired samples did not reveal any recurrent chemotherapy-induced mutations. Gene expression analyses found that most DEGs were upregulated by chemotherapy, primarily in the chemotherapy-resistant specimens. AP-1 transcription factor family genes (*FOS*, *FOSB*, *FRA-1*) were particularly upregulated in chemotherapy-resistant samples. CNV analysis identified recurrent 11q23.1 amplification, which encompasses *SIK2*. *In vitro*, combined treatment with AP-1 or SIK2 inhibitors with carboplatin or paclitaxel demonstrated synergistic effects. These data suggest that AP-1 activity and *SIK2* copy-number amplification are induced by chemotherapy and may represent mechanisms by which chemotherapy resistance evolves in HGSOC. AP-1 and SIK2 are druggable targets with available small molecule inhibitors and represent potential targets to circumvent chemotherapy resistance.

Significance: Genomic and transcriptomic analyses identify increased AP-1 activity and *SIK2* copy-number amplifications in resistant ovarian cancer following neoadjuvant chemotherapy, uncovering synergistic effects of AP-1 and SIK2 inhibitors with chemotherapy.

Introduction

High-grade serous ovarian cancer (HGSOC) is the most common subtype of ovarian cancer with a high mortality rate. In recent years, the paradigm for the treatment of advanced stage HGSOC has shifted from a focus on primary debulking surgery followed by adjuvant chemotherapy to the more frequent use of neoadjuvant chemotherapy (NACT) followed by an interval debulking surgery. This approach has demonstrated non-inferior outcomes with reduced patient morbidity (1). Most large genomic studies of HGSOC, such as The Cancer Genome Atlas (TCGA), have focused on chemotherapy-naïve tumors and therefore cannot assess chemotherapy's impact on the tumor (2). NACT provides an opportunity to better understand the genomic and transcriptomic effects of chemotherapy by enabling direct comparison of paired untreated and treated tumor samples collected from the same patient.

Although HGSOC is one of the most chemotherapy-sensitive solid tumors, with 80% of women responding to their initial treatment, the majority have a recurrence of metastatic disease (3). There is currently no clinically useful way to predict a patient's response to NACT before treatment; however, genomic and transcriptomic studies have begun to reveal the changes that occur following NACT. In a study that compared 10 patients who received NACT with excellent response and 10 patients who received NACT with poor response, nonsense mutations in *CSMD3* and *PIK3CA* were only seen in patients with poor response (4). Transcriptomic analysis of tumors post-NACT has found increased immune cell transcripts compared with pre-NACT samples, suggesting that chemotherapy response is associated with immune recruitment and remodeling (5). A study of patients with matched pre- and post-NACT tumor samples found that pre-NACT transcriptomes were enriched for cell growth pathways and post-NACT transcriptomes for drug transport and peroxisome pathways (6). Another study that employed targeted panel genomic and transcriptomic analyses found that NACT is associated with changes in cell-cycle progression and DNA damage response (7). A study focused on patients with minimal residual disease after NACT demonstrated upregulation of fatty acid oxidation and epithelial-to-mesenchymal transition signature genes in residual tumor cells (8).

We investigated a cohort of matched pre- and post-NACT tumors using RNA sequencing (RNA-seq) and targeted panel DNA sequencing to better understand the effect of NACT on the genome and transcriptome of HGSOC tumors. Our analyses found evidence of transcriptomic remodeling associated with NACT, as well as for genomic instability that gives rise to recurrent amplifications following NACT. This includes the identification of potentially clinically relevant

[1]Department of Obstetrics and Gynecology/Section of Gynecologic Oncology, The University of Chicago, Chicago, Illinois. [2]Department of Pathology, The University of Chicago, Chicago, Illinois. [3]Medicine/Section of Genetic Medicine, The University of Chicago, Chicago, Illinois. [4]MRC Weatherall Institute of Molecular Medicine and Nuffield Department of Women's & Reproductive Health, University of Oxford, Oxford, United Kingdom. [5]Oxford NIHR Biomedical Research Centre, Oxford, United Kingdom.

Note: Supplementary data for this article are available at Cancer Research Online (http://cancerres.aacrjournals.org/).

Corresponding Author: Ernst Lengyel, Department of Obstetrics and Gynecology, University of Chicago, Chicago, IL 60637. Phone: 773-834-0740; E-mail: elengyel@uchicago.edu

Cancer Res 2022;82:169–76

doi: 10.1158/0008-5472.CAN-21-1467

roles for increased AP-1 signaling and *SIK2* amplification in driving the initial responses of tumors to carboplatin and paclitaxel.

Materials and Methods

Clinical cohort

One hundred and fifty-three patients with Federation Internationale de Gynecolgie et d'Obstetrique (FIGO) 2013 advanced stage IIIC or IV HGSOC who received NACT between January 2007 and June 2019 were identified in the University of Chicago (Chicago, IL) ovarian cancer database. In accordance with the Common Rule, all patients in this database provided written informed consent under a University of Chicago Institutional Review Board–approved protocol for use of their archived tissue in future research studies. Fifty patients with high-quality tissue samples collected before and after NACT were selected for analysis. All patients received both carboplatin and paclitaxel for NACT. Patients underwent an interval debulking surgery consisting of hysterectomy, bilateral salpingo-oophorectomy, omentectomy, and other intra-abdominal procedures to remove the maximum amount of tumor. Caucasian women made up the majority of the cohort at 58%, followed by African American women at 28%, Hispanic women at 10%, and Asian women at 4%. Platinum response was defined as resistant if recurrence occurred within 6 months of primary therapy or sensitive if more than 6 months elapsed before disease progression. Pre- and post-chemotherapy samples were submitted to Tempus for DNA and RNA-seq.

Pathologic evaluation and sample preparation

Formalin-fixed paraffin-embedded (FFPE) tissue blocks were cut into 10 μm sections from the patient's pre-NACT biopsy and interval debulking surgery. Samples were assessed by two gynecologic pathologists (R.R. Lastra, D. Chapel) to confirm high-grade histology, stage, and chemotherapy response score (CRS). Samples were also evaluated by a pathologist to ensure at least 20% tumor cellularity and some specimens were macrodissected to increase tumor cellularity. Germline DNA was collected at the time of surgery from peripheral blood mononuclear cells or FFPE sections free of tumor.

DNA and RNA extraction and RNA-seq

Targeted panel sequencing was performed on FFPE samples using the Tempus xT panel, a hybrid capture next-generation sequencing panel that encompasses clinically relevant and known cancer driver genes (Supplementary Table S1). Total tumor nucleic acid was extracted by digesting sections with proteinase K. Each tumor and germline sample had 100 ng of DNA mechanically sheared by a Covaris ultrasonicator to an average size of 200 bp. Libraries were then prepared using KAPA Hyper Prep Kit, hybridized to the xT probe set, and were then amplified with KAPA HiFi HotStart ReadyMix. Remaining nucleic acid was purified to RNA with DNase-I digestion. One-hundred ng of RNA was input to the Kapa RNA Hyperprep kit hybridized to IDT xGen Exome Research Panel version 1 probes. Amplification of cDNA was performed with KAPA HiFi HotStart ReadyMix. Sequencing to an average target depth of 500× was performed on Illumina HiSeq 4000 (version 2) or NovaSeq6000 (version 3). For quality control, each sample was required to have 95% of target bases sequenced to at least 300×.

DNA analysis

Germline data were filtered using the Broad institute hard filter recommendations. Briefly, sequence quality was evaluated by FastQC (v0.11.8, RRID:SCR_014583) and sequences trimmed with Trimmomatic (v0.36, RRID:SCR_011848). Trimmed sample sequence files were mapped to GRCh38 with BWA MEM (v0.7.17, RRID:SCR_010910) and merged. Duplicates were marked with sambamba (v0.6.8) and base quality score recalibration performed using the GATK 4.1.6 tools BaseRecalibrator and ApplyBQSR (RRID:SCR_001876). Germline variants of known clinical interest in ovarian cancer were selected and cBioportal's (SCR_014555) MutationMapper used to generate lollipop plots. Somatic data were annotated with ANNOVAR and reads passing filters were selected for analysis. This included mutations with a variant allele frequency (VAF) of >20% and population variant allele frequency of <5% in women. To estimate mutational burden, exonic single-nucleotide variants with a VAF > 5% that were not in the COSMIC database (RRID:SCR_002260) were included. Copy-number variations (CNV) were detected from panel sequencing data using SynthEx (v1.0.5) and significantly enriched CNVs detected using GISTIC2.0 (v2.0.23, RRID:SCR_000151).

RNA analysis

RNA-seq data were aligned and quantified using Kallisto (v0.46.1, RRID:SCR_016582) against human genome build hg38. Raw counts were normalized using reads per kilobase million (RPKM). Given high interpatient heterogeneity, GFOLD was used to determine which genes were differentially expressed in before and after chemotherapy samples. GFOLD (0.01) was used, meaning in 99% of cases the fold change of a gene is above the calculated GFOLD value. A cut off of >±2 was used to consider expression significantly altered by chemotherapy. STRING database (RRID:SCR_005223) was used for extracting and visualizing gene ontology (GO) terms. R version 4.0.2 (RRID:SCR_000432) with consensusOV package was used to determine molecular subtypes; Complex Heatmap (RRID:SCR_017270) and ggplot2 (RRID:SCR_014601) packages were used for visualizations. Genes in the AP-1 pathway were extracted from the Pathway Interaction Database (PID_AP1_PATHWAY; M167). Kaplan–Meier survival curves were generated with the Kaplan–Meier Plotter using HGSOC datasets GSE14767, GSE15622, GSE18520, GSE19829, GSE23554, GSE26193, GSE26712, GSE26751, GSE30161, GSE3149, GSE51373, GSE63885, GSE65986, GSE9891, and TCGA.

Cell lines and culture conditions

OVCAR-8 cells were obtained from Marcus Peter (Northwestern University, Chicago, IL, RRID: CVCL_IM65), TYK-nu cells from Gottfried Konecny (Ronald Reagan UCLA Medical Center, RRID:CVCL_1776), OVCAR-4 cells from Charles River Fredrick National Laboratory for Cancer Research (RRID:CVCL_1627), and PEO-1 cells from Scott Kaufmann (Mayo Clinic, RRID:CVCL_2686). OVCAR-8 cells were grown in DMEM (10-013-CV; Corning) with 10% FBS (35-010-CV, FBS; Thermo Fisher Scientific), 1% MEM nonessential amino acids (25-025-CI; Corning) and 1% MEM Vitamins (25-020-CI; Corning). TYK-nu cells were grown in MEM (10-022-CV; Corning) with 10% FBS, 1% MEM nonessential amino acids (25-025-CI; Corning), and 1% MEM Vitamins (25-020-CI; Corning). OVCAR-4 cells were grown in RPMI with 10% FBS (35-010-CV, FBS; Thermo Fisher Scientific). PEO-1 cells were grown in DMEM (10-013-CV; Corning) with 10% FBS (35-010-CV, FBS; Thermo Fisher Scientific), 1% MEM nonessential amino acids (25-025-CI; Corning), and 1% MEM Vitamins (25-020-CI; Corning). Cells were grown in 5% CO_2 incubator at 37°C. All cells were *Mycoplasma* negative and their identity verified regularly by short tandem repeat profiling (IDEXX; OVCAR-8 and TYK-nu Feb 2020,

OVCAR-4 June 2019, PEO-1 July 2019). Cells were passaged 2–10 times after unfreezing prior to performing experiments.

Antibodies

c-Jun antibody (1:1,000, ab31419, Abcam, RRID:AB_731605) or c-Jun antibody (1:1,000, 2315, Cell Signaling Technology, RRID: AB_490780), c-Fos antibody (1:500, sc-166940, Santa Cruz Biotechnology, RRID:AB_10609634), anti-thrombospondin 1 (THBS1) antibody (1:100, sc-59887, Santa Cruz Biotechnology, RRID: AB_793045), GAPDH antibody (1:1,000, 2118, Cell Signaling Technology, RRID:AB_561053), SIK2 antibody (1:1,000, 6919S, Cell Signaling Technology, RRID:AB_10830063), phospho-Akt (Ser473) antibody (1:1,000, 9271, Cell Signaling Technology, RRID: AB_329825), and AKT antibody (1:1,000, 9272, Cell Signaling Technology, RRID:AB_329827).

Apoptosis assay with flow cytometry

OVCAR-8 cells (i) treated with 5 μmol/L of SIK2 inhibitor (HG-9-91-01, MedChem Express, HY-15776) for the indicated time, (ii) with stable knockout of *SIK2*, or (iii) OVCAR-8 cells transfected with *SIK2* siRNA or NT siRNA (30 nmol/L; 24 hours, Dharmacon), were treated with carboplatin (100 μmol/L; 72 hours) or paclitaxel (100 nmol/L; 24 hours). Cells were then trypsinized and washed with staining buffer (BD, 554657). A total of 500,000 cells were resuspended in binding buffer (Apoptosis Detection Kit, BioLegend, 640932) and stained with Annexin V (APC) and PI (PE) for 15 minutes at room temperature. Flow cytometry analysis was then carried out using CytoFLEX Flow Cytometer (Beckmann Coulter). Data analysis was carried out using FlowJo 10.7.1 (RRID:SCR_008520).

Proliferation assay

OVCAR-8 cells were seeded at 10,000 cells per well in a black-wall 96-well plate and allowed to adhere for 24 hours before addition of treatment [paclitaxel (100 nmol/L), carboplatin (100 μmol/L), SIK2 inhibitor (5 μmol/L)]. After 24 or 48 hours, nuclei were visualized by addition of Hoechst 33258 (1:5,000) and wells fluorescently imaged with a Nikon Eclipse Ti2 to extract the Hoechst-positive area fraction.

IHC

FFPE tissue sections (5 μm) were deparaffinized with xylene and rehydrated with a graded series of ethanol. For THBS1, the slides were stained using Leica Bond RX automated stainer. Epitope retrieval solution I (Leica Biosystems, AR9640) was used for 20-minute treatment. Anti-THBS1 (1:100) was applied on tissue sections for one-hour incubation and the antigen-antibody binding was detected with Bond polymer refine detection (Leica Biosystems, DS9800). For trichrome stain, slides were placed in Bouin solution at 55°C–66°C for 1 hour and then washed in running water until yellow color disappeared. Next, slides were stained with Weigert Iron Hematoxylin for 3 minutes and washed in running water for 3 minutes. Then, slides were stained with Biebrich Scarlet-Acid Fuschin solution for 3 minutes and rinsed with deionized water. Finally, slides were differentiated in phosphotungstic-phosphomolybdic acid for 3 minutes and immersed slides into aniline blue solution for 5 minutes.

Immunoblotting

Cells were lysed using SDS lysis buffer, and protein estimation was carried out using a BCA Protein Assay Kit (Thermo Fisher Scientific, 23224). Equal protein amounts were resolved using 4%–20% SDS gel and transferred onto nitrocellulose membrane. Signals were detected using 1:3,000 dilutions of either horseradish peroxide–linked anti-mouse (Cell Signaling Technology, 7076, RRID:AB_330924) or anti-rabbit (Cell Signaling Technology, 7074, RRID:AB_2099233) secondary antibodies and subsequently developed with ECL substrate (Bio-Rad, 1705061) or Pico (Thermo Fisher Scientific, 34579). Images were acquired using G: Box (Syngene).

Dual luciferase assay

A total of 200,000 OVCAR-8 cells in 6-well plates were cotransfected with AP-1 reporter (1.5 μg pAP-1-Luc plasmid containing seven AP-1 enhancer elements; Agilent) and pRL-CMV-*Renilla* plasmids (0.1 ng; Promega) using 6 μL of Lipofectamine 2000. Cells were treated with paclitaxel or carboplatin at indicated treatment for 24 hours 2 days after transfection. Cells were lysed, and luminescence measured using a Berthold Technologies Lumat LB 9507 per manufacturer's instructions (Promega Dual Luciferase Reporter Assay).

MTT assay

For inhibitor assays, 10,000 cells were seeded into 96-well plates on day 1 and treated with chemotherapy and inhibitor on day 2. MTT assay (Thiazolyl blue tetrazolium bromide, M2128, Sigma) was performed 72 hours after treatment. TYK-nu and OVCAR-8 cells were treated with constant ratios of drug combinations (carboplatin and SR11302; paclitaxel and SR11302) in serial dilutions and combination indices calculated with Compusyn software.

The data generated in this study are available within the article and its Supplementary Data files. Expression profile data analyzed in this study were obtained from Gene Expression Omnibus at GSE14767, GSE15622, GSE18520, GSE19829, GSE23554, GSE26193, GSE26712, GSE26751, GSE30161, GSE3149, GSE51373, GSE63885, GSE65986, GSE9891.

Results

We identified a cohort of 50 consecutive patients from our ovarian cancer database with advanced stage IIIC and IV HGSOC treated with neoadjuvant carboplatin and paclitaxel. These women were not eligible for primary debulking surgery because of their significant tumor burden on imaging and clinical exam. Tumor tissue was biopsied before NACT and at the interval debulking surgery. After removal of cases that were exceptional responders (9) with minimal tumor tissue at the second surgery and tumors that failed library preparation or sequencing (Materials and Methods), the final patient cohort consisted of 32 paired DNA and 20 paired RNA samples from pre- and post-NACT, with 18 patients contributing both paired DNA and RNA, 14 patients only contributing DNA, and 2 patients only contributing RNA (**Fig. 1A**; Supplementary Fig. S1A; **Table 1**; Supplementary Table S2 and S3).

Three patients (10%) carried a BRCA1 and 1 patient (4%) a BRCA2 germline mutation (Supplementary Fig. S1B); both BRCA1 patients were chemotherapy sensitive and the BRCA2 patient was chemotherapy resistant. Patients were nearly evenly split between platinum sensitive (>6 months to recurrence after the end of chemotherapy) and resistant (<6 months to recurrence) disease. Whole transcriptome t-SNE analysis established that clustering of samples was driven by pre- or post-chemotherapy status, but not chemotherapy sensitivity (**Fig. 1B**). Increased epithelial marker expression was not correlated with a lower pathologic tumor content (Supplementary Fig. S1C). We determined each patient's TCGA molecular subtype (10) pre- and post-NACT and found that 50% of patients underwent a subtype change (**Fig. 1C**) consistent with previous reports (6). There

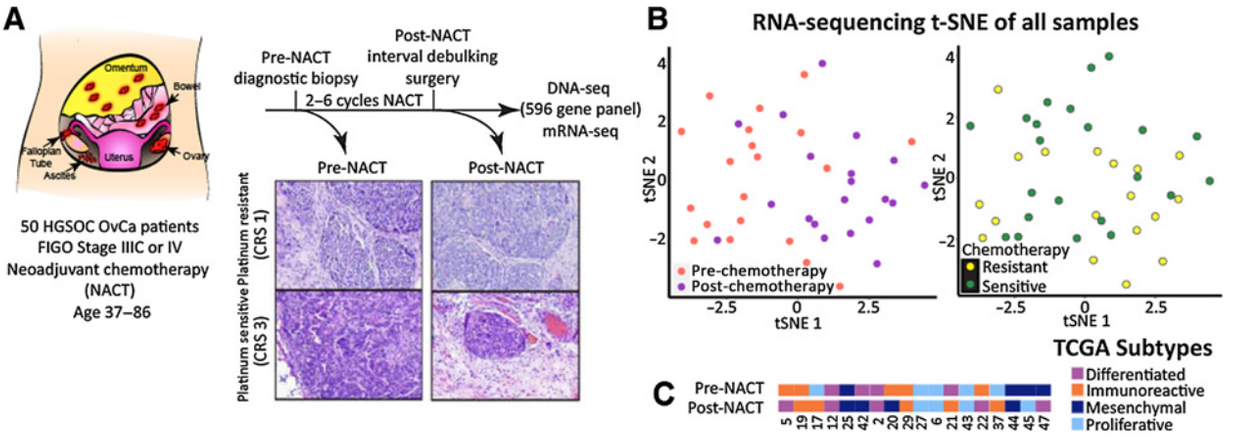

Figure 1.

Transcriptomic and genomic characterization of HGSOC response to NACT. **A,** Overview of cohort and sample collection time points. Representative hematoxylin and eosin of matched pairs of pre- and post-NACT samples from tumors with poor pathologic response to therapy (CRS 1) or excellent response to therapy (CRS 3; ×40 magnification). **B,** RNA-seq of whole transcriptome showed that samples cluster based on treatment status (pre- or post-NACT) rather than chemosensitivity, as visualized with t-SNE. CRS, chemotherapy response score; t-SNE, t-distributed stochastic neighbor embedding. **C,** Molecular subtype (2) of indicated patients before and after NACT. Patient molecular subtypes are plastic and frequently change after NACT.

was no correlation between chemotherapy resistance and pre-NACT TCGA subtype ($P = 0.9$), post-NACT subtype ($P = 0.4$), or change in subtype ($P = 0.6$). As HGSOC molecular subtypes were initially identified from chemotherapy-naïve patient specimens and are imperfect prognostic indicators (2), these data suggest that tumors are highly plastic and surviving tumor cells adapt to chemotherapy by changing gene expression (11).

Table 1. Clinical characteristics of the NACT HGSOC patient cohort.

Characteristics, *n* (%)	DNA-seq patients (32)	RNA-seq patients (20)
Median age at diagnosis, years (range)	60 (43–86)	61 (46–80)
Median cycles of neoadjuvant chemotherapy (range)	3 (3–6)	3 (3–4)
FIGO stage		
IIIC	21 (66%)	16 (80%)
IVA	2 (6%)	0
IVB	9 (28%)	4 (20%)
Primary disease site		
Ovary	17 (53%)	12 (60%)
Fallopian tube	15 (47%)	8 (40%)
Peritoneum	0	0
Tumor debulking status		
Optimal	26 (81%)	16 (80%)
Suboptimal	6 (19%)	4 (20%)
Chemotherapy response score[a]		
1	15 (48%)	8 (42%)
2	8 (26%)	7 (37%)
3	8 (26%)	4 (21%)
Primary platinum response		
Sensitive	18 (56%)	12 (60%)
Resistant	14 (44%)	8 (40%)
Median progression-free survival, days (range)	460 (246–1,693)	521 (199–1,257)
Median overall survival, days (range)	734 (292–2,248)	720 (292–2,248)

[a]One patient with unknown score.

Analyzing all patients, 77 genes were upregulated after chemotherapy and 15 genes were downregulated (**Fig. 2A**). To identify differentially expressed genes (DEG) associated with chemotherapy response, we performed a paired analysis of each patient's pre- and post-NACT sample using GFOLD (Supplementary Tables S4–S8). When samples were clustered on the basis of read counts, clustering occured by before or after chemotherapy status and not chemotherapy response. However, when clustering was based on DEGs, the samples did cluster by response as well as chemotherapy status (**Fig. 2A**; Supplementary Fig. S2A). We validated previous observations that *FOS*, *NR4A1*, *NR4A3*, *NTRK2*, *SFRP2*, and *SFRP4* are upregulated following NACT (7). When categorizing patients by platinum sensitivity, we identified 141 genes exclusively upregulated in chemotherapy-resistant patients compared with only seven genes in chemotherapy-sensitive patients (Supplementary Table S9), consistent with findings in triple-negative breast cancer that shares many genomic features with HGSOC (12). Genes downregulated following NACT included several genes associated with DNA replication and the cell cycle (e.g., *MKI67*, *MCM10*, *TOP2A*, and *CENP*). Upregulated genes included extracellular matrix genes (e.g., *COL14A1*, *THBS1*; **Fig. 2B**), metabolic genes (e.g., *ALDH1A1*, *FABP4*, *AOX1*), cytokines (e.g., *CCL14* and *IL6*), and transcriptional regulators. In particular, genes involved in the AP-1 transcription factor network, including *FOS*, *FOSL1*, and *FOSB*, showed consistently high expression following NACT (**Fig. 2C**; Supplementary Fig. S2B and S2C). Supporting a functional role of AP-1 family members in chemotherapy resistance, we found that the core AP-1 genes were more highly expressed in chemoresistant patients (Supplementary Fig. S2D; Supplementary Table S10). Consistent with our findings, Jiménez-Sánchez and colleagues (5) identified similar increases in the expression of AP-1 pathway genes in platinum resistant patients following chemotherapy using a microarray (Supplementary Fig. S2E).

On the basis of the consistently elevated expression of AP-1 family members in the chemoresistant post-treatment samples, we further investigated their functional role in mediating chemoresistance. The activator protein 1 (AP-1) transcription factor is a dimeric leucine-

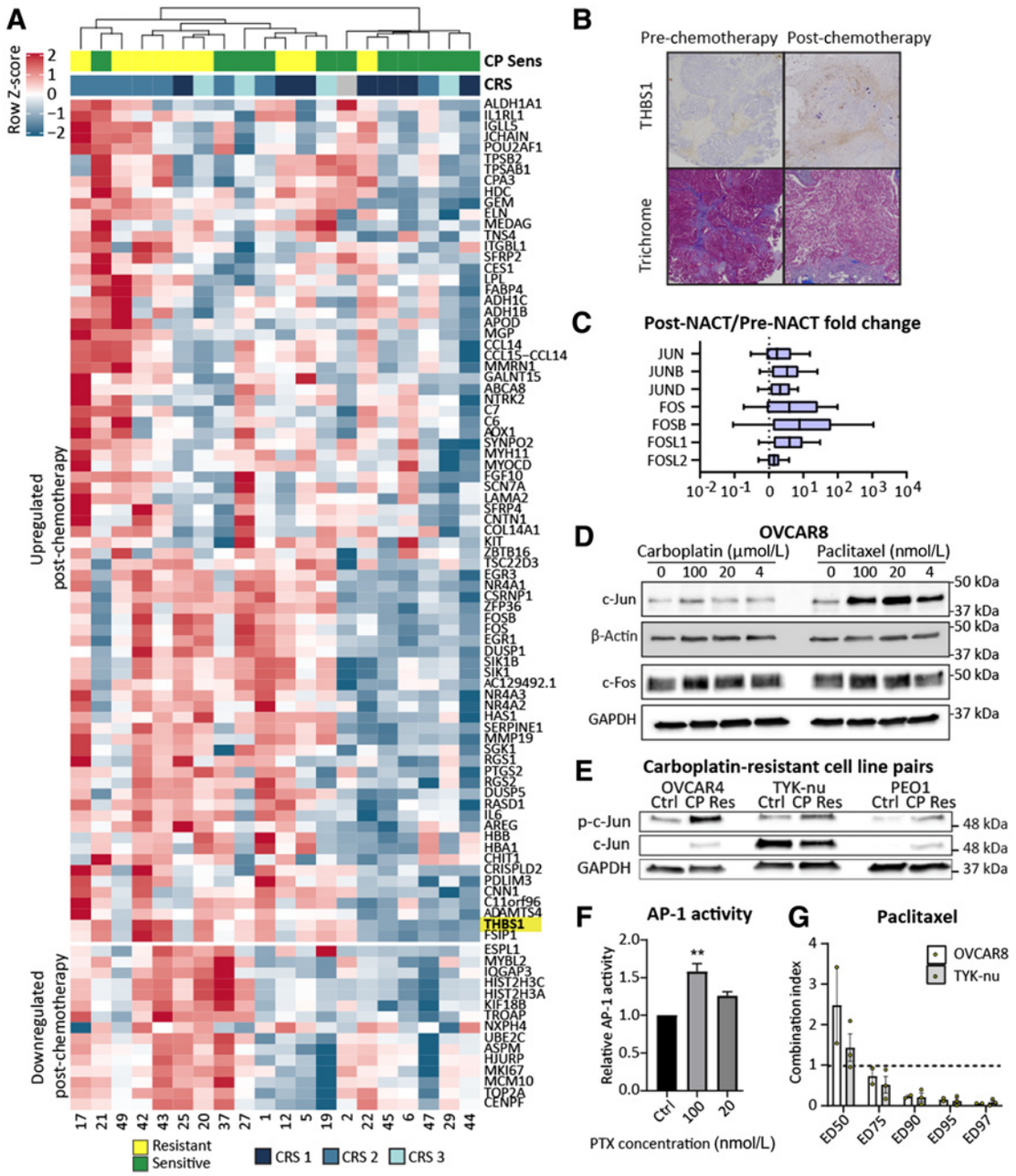

Figure 2.

NACT is associated with increased AP-1 activity. **A,** Hierarchical clustering of DEGs following NACT (>±2 GFOLD) finds that patients cluster by platinum sensitivity. **B,** Pre- and post-chemotherapy IHC (×40) demonstrating increased THBS1 (thrombospondin) expression after chemotherapy. THBS1 is an extracellular matrix protein whose gene expression is upregulated after chemotherapy, as highlighted in **Fig. 1A**. Trichrome staining demonstrates stable quantity of blue staining collagen regardless of chemotherapy status. **C,** Expression of core AP-1 transcription factors is consistently elevated after NACT, including *c-Jun* and *c-Fos*. **D,** Treatment of OVCAR-8 cells with paclitaxel, but not carboplatin, for 24 hours leads to a dose-dependent increase in c-Jun protein levels. c-Fos levels were unaffected. **E,** On immunoblot carboplatin (CP)-resistant OVCAR-4, TYK-nu, and PEO1 cells have elevated levels of phosphorylated c-Jun (Ser63) compared with control cells. **F,** AP-1 transcriptional activity as assessed with a luciferase reporter plasmid incorporating multiple AP-1 binding sites was increased in OVCAR-8 cells following treatment with paclitaxel at the indicated concentrations for 24 hours. **G,** Combination of PTX with the AP-1 inhibitor SR11302 leads to synergistic cytotoxicity of OVCAR-8 and TYK-nu cells at large effect sizes (ED, effective dose; ED_{75}-ED_{97}). Combination index of less than 1 indicates synergistic activity of AP-1 inhibitor with paclitaxel. CP sens, platinum sensitive. ANOVA, **, $P < 0.01$.

zipper protein composed of elements from the JUN, FOS, ATF, and MAF protein families, which play important roles in cell proliferation and invasion (13). While AP-1 expression is predominantly tumor promoting, some family members can act as tumor suppressors depending on heterodimer composition, cell type, and tumor microenvironment (14). Treatment of HGSOC cell lines with carboplatin and paclitaxel led to an increase in total and phosphorylated c-Jun (**Fig. 2D**; Supplementary Fig. S3A and S3B). Platinum-resistant cell lines generated by long-term, *in vitro* treatment of OVCAR-4, TYK-nu, and PEO1 cells with carboplatin had significantly elevated levels of c-Jun phosphorylation (**Fig. 2E**). Paclitaxel, but not carboplatin, increased AP-1 transcriptional activity, as assessed with a luciferase reporter system (**Fig. 2F**; Supplementary Fig. S3C). Treatment of ovarian cancer cells with an AP-1 inhibitor [SR11302 (15)] combined with paclitaxel or carboplatin led to a synergistic increase in cell death (**Fig. 2G**; Supplementary Fig. S3D), which was present at lower kill fractions for paclitaxel than carboplatin. Moreover, elevated expression of both *c-Jun* and *c-Fos* are consistently associated with worse overall and progression-free survival in several large-scale transcriptomic analyses of patients with epithelial ovarian cancer (Supplementary Fig. S3E–S3H). Combined, these data suggest that both carboplatin and taxane-based chemotherapies select cells with elevated AP-1 transcriptional activity.

Panel sequencing of cancer-associated genes identified between one and 14 nonsynonymous mutations per patient; 12 genes were mutated in 2 or more patients (**Fig. 3A**; Supplementary Tables S11 and S12). No gene demonstrated a recurrent gain in mutation following NACT, suggesting that NACT does not recurrently alter specific genes. There were no significant differences in average mutational burden pre- and post-NACT and mutational burden was not associated with chemotherapy resistance or CRS (Supplementary Fig. S4A). Patients showed both an increase and decrease in mutational burden following NACT, which is in contrast to breast cancer, which demonstrates either no change or decrease in mutations (16). Consistent with other studies, we found that the most common mutational class was driven by the aging-related C>T transition signature caused by spontaneous deamination of 5-methylcytosine (**Fig. 3B**; ref. 9). As expected, *TP53* mutations were the primary recurrent mutation found, identified in all but 1 patient. Consistent with TCGA and other analyses, we identified mutations in *NF1* (9%), *BRCA1* (3%), and *BRCA2* (3%) (2) in several patients; other mutations present in multiple patients included *APOB*, *MTOR*, *CREBBP*, *NRG1*, *PAX3*, and *SALL2*. Reduced *NF1* expression is associated with decreased 5-year survival and chemotherapy resistance in multiple cancer types, while *APOB* (9%) is recurrently mutated in hepatocellular carcinoma, and *MTOR* (9%) mutations are common in renal cell cancers. *CREBBP* mutations in acute lymphoblastic leukemia, *NRG1* fusions in non–small cell lung cancer, *PAX3* overexpression in gliomas, and epigenetic silencing of *SALL2* in breast cancer are all genomic events that have been associated with chemotherapy resistance (17).

Copy-number profiles of patient samples generally recapitulated those identified in TCGA and other analyses (2), with frequent amplification of chromosome 3q and 8q and deletion of chromosomes 16 and 17 (**Fig. 4A**; Supplementary Table S13). In general, both pre- and post-NACT specimens were characterized by widespread genomic instability. To identify recurrently amplified and deleted chromosomal regions, we performed CNV analysis with GISTIC2.0 (18) software tool. We identified several regions that were recurrently amplified or deleted following NACT, emphasizing that NACT leads to the induction or selection of conserved copy-number alterations in HGSOC. The most prominent were amplification of 2q33.1 and 11q23.1 and deletion of 19p13.3 and 2q35 (**Fig. 4B**). Relatively few to no copy-number gains or losses were associated with response to NACT or associated with recurrence 1 year after NACT, independent of whether pre- or post-NACT samples were interrogated (Supplementary Fig. S4B). The most significant amplification was noted in 11q23.1, which encompasses salt-inducible kinase 2 (*SIK2*), a serine/threonine kinase that is associated with paclitaxel and platinum resistance in ovarian cancer (19, 20) (Supplementary Table S14). Genomic amplification of *SIK2* has not been described as a mechanism driving SIK2 upregulation, but our analysis shows that the expression of *SIK2* is strongly associated with copy-number status ($P < 0.0001$; **Fig. 4C**; Supplementary Fig. S4C). The treatment of OVCAR-8 HGSOC cells with carboplatin or paclitaxel and a SIK2 inhibitor led to a significant synergistic increase in cell death (**Fig. 4D**). Addition of SIK2 inhibitor HG-9–91–01 (19) or blocking *SIK2* with siRNA against *SIK2* inhibited AKT activity (Supplementary Fig. S4D). Genomic amplification of *SIK2* in response to NACT may be a novel mechanism by which HGSOC evolves resistance to cytotoxic therapies.

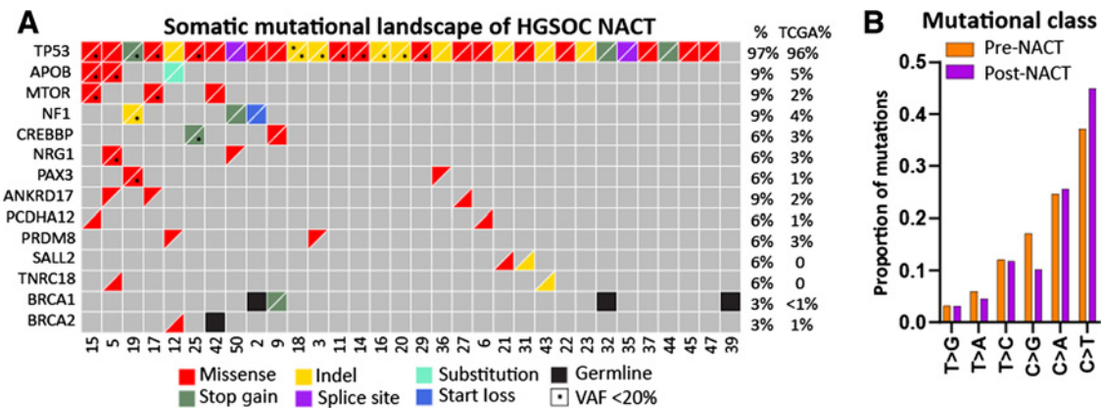

Figure 3.

NACT is not associated with the acquisition of somatic mutations. **A,** Oncoprint of all somatic mutations detected in at least two patient samples. Left upper triangle in each square corresponds to pre-NACT sample and right lower triangle corresponds to post-NACT tissue. Mutational types are indicated by color. The frequency of mutations within our cohort is compared with the frequency of mutations in TCGA analysis of HGSOC. VAF, variant allele frequency. **B,** Proportion of each mutational class in all coding genes detected in the entire patient cohort, divided on the basis of pre or post-NACT.

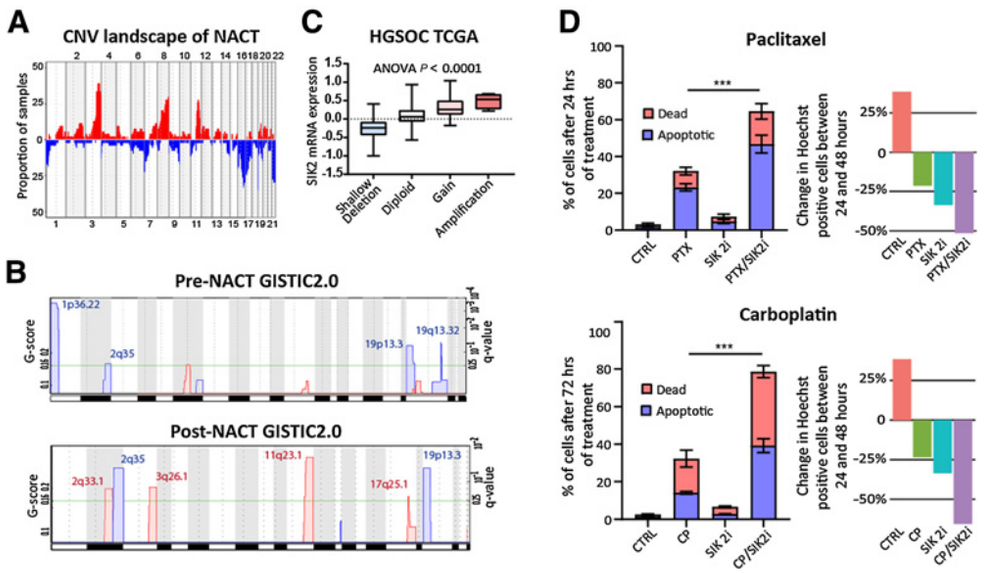

Figure 4.

Recurrent CNVs associated with NACT. **A,** The frequency of CNVs in the patient cohort captures recurrent CNVs observed in TCGA analysis of HGSOC such as amplification of 3q and 8q and deletion of chromosomes 16 and 22. **B,** Comparing TCGA HGSOC cohort normalized *SIK2* mRNA expression with copy-number alteration data reveals increased SIK2 expression with copy-number gain or amplification. **C,** GISTIC2.0 analysis of differentially amplified (red) and deleted (blue) regions identifies recurrent CNVs present both pre- and post-NACT, including frequent amplification of *SIK2* in 11q23.1, which contains 75 total genes (Supplementary Table S14). Chromosome locations are indicated on the *x*-axis. **D,** Treatment of OVCAR-8 cells with a combination of paclitaxel (PTX, 100 nmol/L) or carboplatin (CP, 100 μmol/L) and a SIK2 inhibitor (SIK2i; HG-9-91-01; 5 μmol/L) leads to synergistic cytotoxicity based on two-way ANOVA and Tukey test. Proliferation data demonstrating percent change in the Hoechst-positive area between the 24 and 72 hours after treatment time points is shown in the panels on the right. ANOVA, ***, $P < 0.001$.

Discussion

Using a combination of transcriptomic and genomic analyses, we found that NACT is associated with significant transcriptomic remodeling, including upregulation of AP-1 transcriptional networks. Although tumors continue to evolve mutations during NACT, no recurrently mutated genes associated with NACT were identified in our patient cohort. In contrast, we found evidence that NACT is associated with recurrent copy-number alterations, including amplification of 11q23.1, which is associated with increased expression of SIK2. The selection criteria for NACT is inconsistent, but patients triaged to NACT typically have a higher disease burden, increased ascites, and are more medical complex than primary debulking surgery candidates (1). Although our study provides insight into the molecular mechanisms underlying chemotherapy response in HGSOC, fully understanding the adaptive and evolutionary processes underlying the response of tumor cells to NACT will require an analysis of clonal dynamics and epigenetic processes. In particular, single-cell techniques will be useful to understand NACT-associated transcriptional remodeling by unraveling the selection pressure of NACT on pre-existing tumor cell populations from the induction of specific gene expression programs in tumor cells (or stromal) subpopulations.

Our data suggest that AP-1 activity is induced by chemotherapy and may contribute to the survival of cancer cells in response to cytotoxic agents. AP-1 is a druggable target for which multiple classes of small-molecule inhibitors have been developed. Several AP-1 inhibitors have undergone clinical testing for inflammatory conditions, including rheumatoid arthritis. Therefore, it is possible to consider therapeutically targeting AP-1 in the context of NACT for the purpose of overcoming chemoresistance. In addition, work from our group and others have demonstrated that SIK2 is a therapeutically tractable mediator of platinum and paclitaxel sensitivity in ovarian cancer. Indeed, a small-molecule inhibitor of SIK2 (GRN-300) is currently under investigation for the treatment of recurrent ovarian, primary peritoneal, and fallopian tube cancers (NCT04711161).

Authors' Disclosures

M. Javellana reports nonfinancial support from Tempus during the conduct of the study. J. Heide reports grants from DFG (German Research Foundation) during the conduct of the study. D.B. Chapel reports grants from Ovarian Cancer Research Alliance outside the submitted work. S. Yamada reports other support from Bears Care and Harris Family during the conduct of the study and personal fees from ABOG outside the submitted work. A.A. Ahmed reports personal fees from Singula Bio Ltd outside the submitted work. E. Lengyel reports other support from Tempus during the conduct of the study and grants from AbbVie and Arsenal Bioscience outside the submitted work. No disclosures were reported by the other authors.

Authors' Contributions

M. Javellana: Conceptualization, data curation, formal analysis, investigation, visualization, writing–original draft. **M.A. Eckert:** Conceptualization, formal analysis, supervision, funding acquisition, investigation, visualization, writing–original draft. **J. Heide:** Investigation, writing–original draft. **K. Zawieracz:** Investigation, writing–review and editing. **M. Weigert:** Investigation, writing–review and editing. **S. Ashley:** Investigation. **E. Stock:** Investigation, writing–review and editing. **D. Chapel:** Investigation, writing–review and editing. **L. Huang:** Software, formal analysis. **S.D. Yamada:** Writing–review and editing. **A.A. Ahmed:** Investigation, writing–review and editing. **R.R. Lastra:** Investigation, writing–review and editing. **M. Chen:** Software, formal analysis, supervision, writing–review and editing. **E. Lengyel:** Conceptualization, resources, supervision, funding acquisition, writing–review and editing.

Acknowledgments

The authors thank Gail Isenberg for help with editing the article. They appreciate Martin Miller Ph.D. Cancer Systems Biology Lab, CRUK, Cambridge University for sharing RNA-seq results. This project was supported by a grant from the NCI (R01CA169604 to E. Lengyel) and funding from Tempus for panel sequencing (E. Lengyel and M. Eckert).

The costs of publication of this article were defrayed in part by the payment of page charges. This article must therefore be hereby marked *advertisement* in accordance with 18 U.S.C. Section 1734 solely to indicate this fact.

Received May 11, 2021; revised September 12, 2021; accepted October 29, 2021; published first November 4, 2021.

References

1. Vergote I, Coens C, Nankivell M, Kristensen GB, Parmar MKB, Ehlen T, et al. Neoadjuvant chemotherapy versus debulking surgery in advanced tubo-ovarian cancers: pooled analysis of individual patient data from the EORTC 55971 and CHORUS trials. Lancet Oncol 2018;19:1680–7.
2. Cancer Genome Atlas Research Network. Integrated genomic analyses of ovarian carcinoma. Nature 2011;474:609–15.
3. Bowtell DD, Bohm S, Ahmed AA, Aspuria PJ, Bast RC Jr, Beral V, et al. Rethinking ovarian cancer II: reducing mortality from high-grade serous ovarian cancer. Nat Rev Cancer 2015;15:668–79.
4. Lee S, Zhao L, Rojas C, Bateman NW, Yao H, Lara OD, et al. Molecular analysis of clinically defined subsets of high-grade serous ovarian cancer. Cell Rep 2020;31: 107502.
5. Jiménez-Sánchez A, Cybulska P, Mager KL, Koplev S, Cast O, Couturier D-L, et al. Unraveling tumor–immune heterogeneity in advanced ovarian cancer uncovers immunogenic effect of chemotherapy. Nat Genet 2020;52:582–93.
6. Glasgow MA, Argenta P, Abrahante JE, Shetty M, Talukdar S, Croonquist PA, et al. Biological insights into chemotherapy resistance in ovarian cancer. Int J Mol Sci 2019;20:2131.
7. Arend RC, Londono AI, Montgomery AM, Smith HJ, Dobbin ZC, Katre AA, et al. Molecular response to neoadjuvant chemotherapy in high-grade serous ovarian carcinoma. Mol Cancer Res 2018;16:813–24.
8. Artibani M, Masuda K, Hu Z, Rauher PC, Mallett G, Wietek N, et al. Adipocyte-like signature in ovarian cancer minimal residual disease identifies metabolic vulnerabilities of tumor-initiating cells. JCI Insight 2021;6:e147929.
9. Patch AM, Christie EL, Etemadmoghadam D, Garsed DW, George J, Fereday S, et al. Whole-genome characterization of chemoresistant ovarian cancer. Nature 2015;521:489–94.
10. Chen GM, Kannan L, Geistlinger L, Kofia V, Safikhani Z, Gendoo DMA, et al. Consensus on molecular subtypes of high-grade serous ovarian carcinoma. Clin Cancer Res 2018;24:5037–47.
11. Drapkin BJ, Minna JD. Studying lineage plasticity one cell at a time. Cancer Cell 2020;38:150–2.
12. Berger AC, Korkut A, Kanchi RS, Hegde AM, Lenoir W, Liu W, et al. A comprehensive pan-cancer molecular study of gynecologic and breast cancers. Cancer Cell 2018;33:690–705.
13. Lengyel E, Wang H, Stepp E, Juarez J, Wang Y, Doe W, et al. Requirement of an upstream AP-1 motif for the constitutive and phorbol ester-inducible expression of the urokinase-type plasminogen activator receptor gene. J Biol Chem 1996; 271:23176–84.
14. Eferl R, Wagner EF. AP-1: a double-edged sword in tumorigenesis. Nat Rev Cancer 2003;3:859–68.
15. Mishra DK, Kim MP. SR 11302, an AP-1 inhibitor, reduces metastatic lesion formation in *ex vivo* 4D lung cancer model. Cancer Microenviron 2017;10: 95–103.
16. Kim C, Gao R, Sei E, Brandt R, Hartman J, Hatschek T, et al. Chemoresistance evolution in triple-negative breast cancer delineated by single-cell sequencing. Cell 2018;173:879–93.
17. Cancer Genome Atlas Research Network, Weinstein JN, Collisson EA, Mills GB, Shaw KR, Ozenberger BA, et al. The cancer genome atlas pan-cancer analysis project. Nat Genet 2013;45:1113–20.
18. Mermel CH, Schumacher SE, Hill B, Meyerson ML, Beroukhim R, Getz G. GISTIC2.0 facilitates sensitive and confident localization of the targets of focal somatic copy-number alteration in human cancers. Genome Biol 2011;12:R41.
19. Miranda F, Mannion D, Liu S, Zheng Y, Mangala LS, Redondo C, et al. Salt-inducible kinase 2 couples ovarian cancer cell metabolism with survival at the adipocyte-rich metastatic niche. Cancer Cell 2016;30:273–89.
20. Ahmed AA, Lu Z, Jennings NB, Etemadmoghadam D, Capalbo L, Jacamo RO, et al. SIK2 is a centrosome kinase required for bipolar mitotic spindle formation that provides a potential target for therapy in ovarian cancer. Cancer Cell 2010; 18:109–21.